remote sensing

Article

Land Subsidence Phenomena vs. Coastal Flood Hazard—The Cases of Messolonghi and Aitolikon (Greece)

Nikolaos Antoniadis [1], Stavroula Alatza [2], Constantinos Loupasakis [1,*] and Charalampos (Haris) Kontoes [2]

[1] School of Mining and Metallurgical Engineering, Department of Geological Sciences, Zographou Campus, National Technical University of Athens, GR-157 80 Athens, Greece
[2] National Observatory of Athens (NOA), Operational Unit BEYOND Centre for Earth Observation Research and Satellite Remote Sensing, Institute for Astronomy, Astrophysics, Space Applications and Remote Sensing, GR-152 36 Athens, Greece
* Correspondence: cloupasakis@metal.ntua.gr

Abstract: Land subsidence in coastal and delta cities often results in infrastructure and residential building damages, while also increasing the area's flooding vulnerability. The coastal cities of Messolonghi and Aitolikon are typical examples, as they are built on top of old stream deposits near the coast. In the last several years, the gradual subsidence of the sites, combined with the impact of climate change, resulted in multiple floods. The rush of seawater over the lowlands has also been reported. Persistent scatterer interferometry (PSI) is a remote-sensing technique that can provide a reliable and cost-effective solution, as it can be used to identify and monitor soil displacements. In this study, a novel parallelized PSI (P-PSI) processing chain, developed by the Operational Unit Center for Earth Observation Research and Satellite Remote Sensing (BEYOND) of the National Observatory of Athens, as well as the Copernicus EGMS product were used to identify these displacements. The results were examined in correlation with other potential factors such as the overexploitation of the underground water, the natural compaction of the clay soil layers, the primary and secondary consolidation due to the external construction loading, the oxidation of the organic soils, tidal gauge data, precipitation data, and ground truth data. In Messolonghi, various deformation rates were recorded, with maximum mean values of −5 mm/year in the eastern part, whereas in Aitolikon, the maximum values were around −4.5 mm/year. The displacements were mostly attributed to the primary consolidation due to the building loads. Deformation patterns and their correlation with precipitation could also be witnessed. It was evident that the increased precipitation rates and sea level rise played a leading role in the constant flooding.

Keywords: geohazards; land subsidence; flooding; remote sensing; ground truth data; persistent scatterer interferometry; InSAR; European Ground Motion Service; Copernicus Land Monitoring Service; climate change; Messolonghi; Aitolikon

check for updates

Citation: Antoniadis, N.; Alatza, S.; Loupasakis, C.; Kontoes, C. Land Subsidence Phenomena vs. Coastal Flood Hazard—The Cases of Messolonghi and Aitolikon (Greece). *Remote Sens.* **2023**, *15*, 2112. https://doi.org/10.3390/rs15082112

Academic Editors: Zhong Lu, Alex Hay-Man Ng, Raffaele Albano, Dimitrios D. Alexakis, Maria Ferentinou and Christos Polykretis

Received: 7 December 2022
Revised: 4 April 2023
Accepted: 10 April 2023
Published: 17 April 2023

1. Introduction

Land subsidence is a major threat in urban areas. Continuous vertical displacements over time can severely damage linear infrastructures, such as bridges, road networks, railways, and pipelines, and create serious building stability problems when differential settlements occur [1–3]. This ground deformation phenomenon may occur as a consequence of natural processes, such as organic soils oxidation [4,5], the collapse of underground cavities [6–8], and natural compaction [9], or due to anthropogenic processes, such as groundwater overexploitation [10–15] or as a combination of both natural and anthropogenic processes. The relevant international literature has focused on studying tectonic structures, karst, and the extraction of fluids from the subsoil as causes of land subsidence. Thus, natural causes—those related to the nature of recent sediments, such as subsurface stratigraphic architecture and primary and secondary consolidation—are not widely investigated. Nevertheless, land subsidence caused by natural causes has been observed and studied in other areas of the Mediterranean and internationally [16–21].

Another phenomenon manifested in coastal areas and presented in this study is flooding. Sea level rise (SLR) accompanying climate change has begun to cause significant damage in coastal areas around the world [22–24].

The detection, measurement, and monitoring of land subsidence are crucial for both urban areas and infrastructures. Interferometric Synthetic Aperture Radar (InSAR) is a well-established method for monitoring ground displacement phenomena and is successfully applied in a variety of Earth deformation studies around the world [25–31] and Greece [32–38]. Numerous land subsidence sites in Greece have been detected and analyzed using InSAR techniques. Land subsidence case studies worth mentioning are the Thessaly plain in central Greece [39–41], the wider area close to the Kalochori and Sindos villages west of the Thessaloniki plain [42–45], and the Anthemountas basin east of the Thessaloniki city [46–51].

The current study focused on land subsidence phenomena along the coastal areas of Messolonghi and Aitolikon (Figure 1a) during the last decade, using the Persistent Scatterer (PSI) interferometry technique.

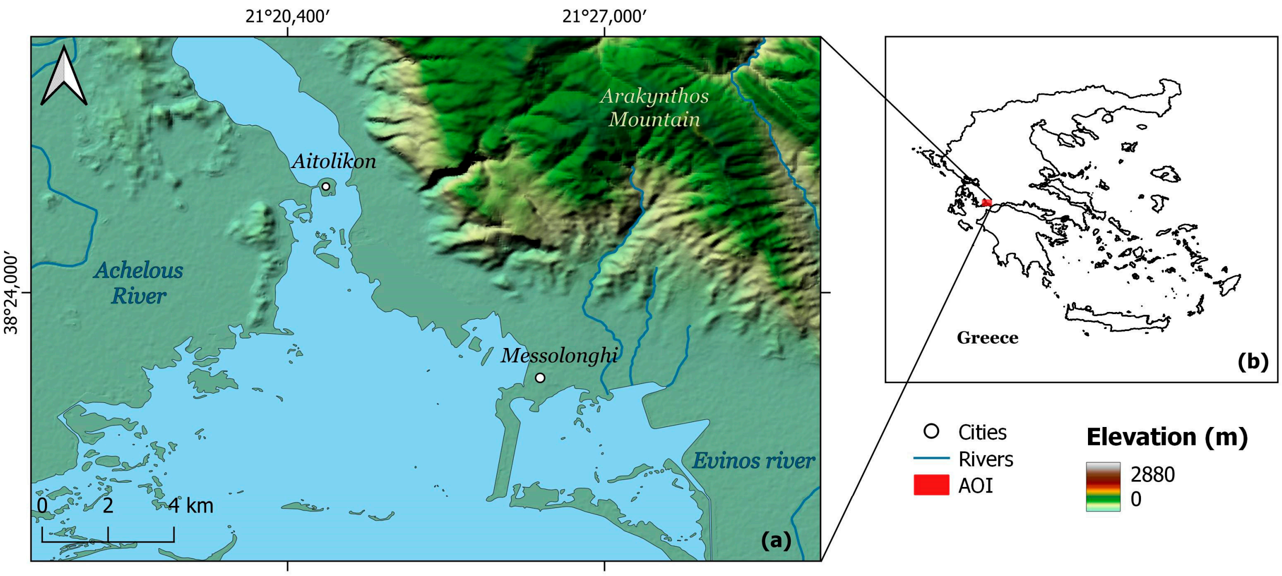

Figure 1. (**a**) The cities of Messolonghi and Aitolikon & (**b**) Location of study area.

The city of Messolonghi is surrounded by the homonymous sea lagoon. It is considered one of Europe's ecologically and environmentally most significant sea lagoons, home to a wide variety of rare plants and animals. The surrounding area consists primarily of cultivated land, while some swamps and saline soils can be seen around the lagoon and along the river deltas. Sandy islets on the front of the lagoons are a particularly sensitive morphological element crucial for preserving the lagoon system.

Aitolikon is situated in the center of the Aitolikon Lagoon, 10 kilometers northeast of Messolonghi. Two 19th-century stone arched bridges, each approximately 300 m long, connect it to the shore on both the east and west sides. Aitolikon initially consisted of 4–5 very small islands in the center of a lagoon, which were completely submerged during the winter. The first attempts to link the islands were conducted by fishermen using wooden piles and earth fills. Over the years, continuous filling was added, resulting in the formation of an irregularly shaped island 300 m in diameter. The last filling was added in 1969, with particular attention paid to the north and south sides. The addition of fillings enabled the building of more houses in the reclaimed area. However, the north side especially presented major problems as the buildings' foundations were under the water.

Over the past few years, flooding and building damage have been reported in these rural areas. To our knowledge, no previous holistic research pertaining to surface deformations and their causes has been conducted. The study area is a densely populated environment. As such, it is vulnerable and carries a significant risk from this geohazard.

The primary scope of the present study is to detect and investigate land subsidence phenomena in Messolonghi and Aitolikon areas using remote sensing techniques and ground truth data. The Persistent Scatterers interferometry technique was implemented in Sentinel-1 SLC images from 2015 to 2021 to perform a time series analysis of the line-of-sight (LOS) displacements in the affected areas. The parallelized PSI (P-PSI) processing chain [52], developed in the Operational Unit BEYOND Center for EO Research and Satellite Remote Sensing of the National Observatory of Athens (NOA), was used for the processing of SAR data and the extraction of the LOS deformation field. The estimated LOS displacements verified the land subsidence phenomena in both sites. The velocities of permanent scatterers, combined with the geological, geotechnical, and hydrogeological data, validated the observed Permanent Scatterers' negative velocities and enabled a more accurate interpretation of the phenomenon.

2. The Study Area

2.1. Geological Setting

Regarding the geological setting of Messolonghi, the city occupies a flat lowland and is founded on Quaternary alluvial deposits consisting of fine grain sediments (clays, silts, and sands).

The stream of Agrilia, originating from the Arakynthos mountain, has been the main provider of fluvial deposits of the Messolonghi narrow site. Currently, the stream travels along its natural course until it is forced to loop around the city (Figure 2). It is believed that the area's first settlers changed the course of the river, preventing the city from flooding. The stream's estimated natural flow network before the area was settled is shown on the map of Figure 2, with red dashed lines. Under natural conditions, the compaction in deltaic areas is counterbalanced by the deposition of sediments transported by the rivers and streams, especially during significant floods. In this case, diverting the stream has prevented the river sediments from reaching the coastal areas, and thus the natural land subsidence has not been offset by the sediment accumulation.

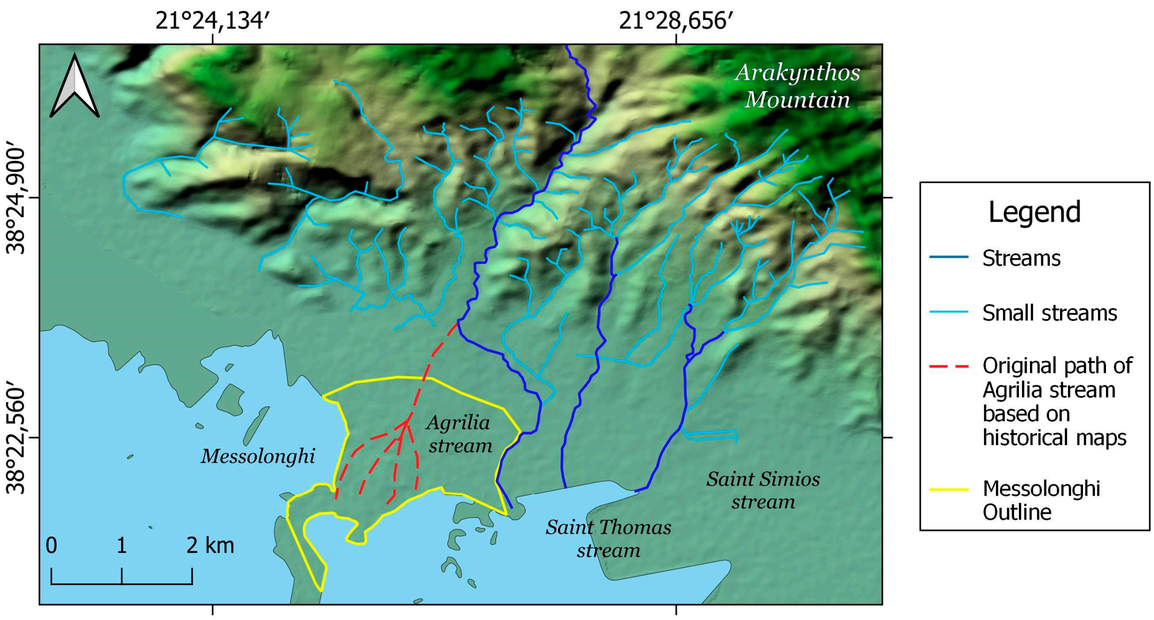

Figure 2. Hydrographical map of Messolonghi greater area.

According to data obtained from geotechnical boreholes, the Quaternary formations consist of recent alluvial deposits (Figure 3). The loose Quaternary coastal deposits extend horizontally along the site consisting of soft clay horizons intercalated with sandy silt to silty sand and silt, reaching down to a maximum depth of approximately 100 m.

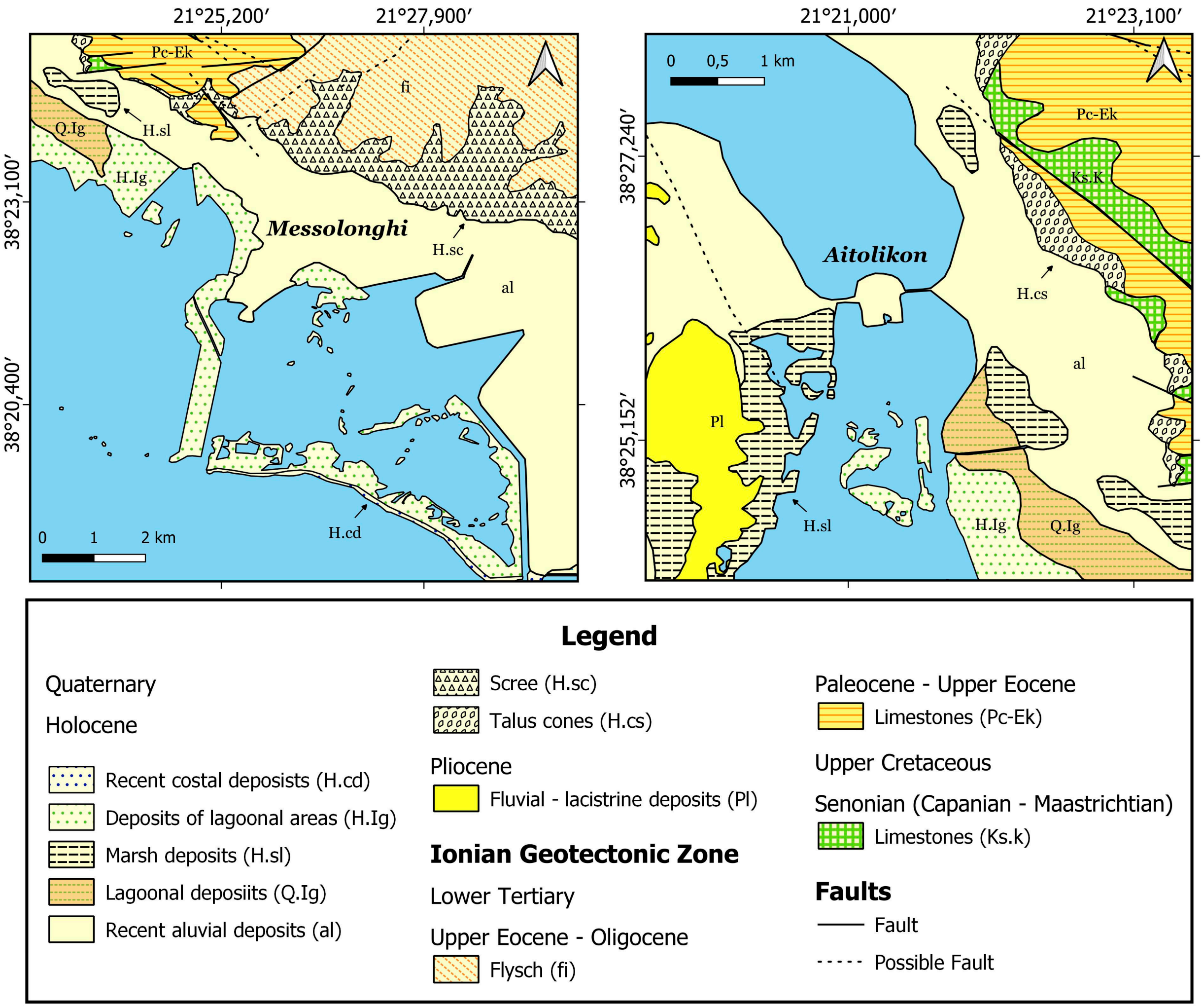

Figure 3. Geological maps of the Messolonghi (**left**) and Aitolikon (**right**) modified by Hellenic Survey of Geology & Mineral Exploration (HSGME) (1987–1990).

Focusing on the top layers bearing loads of the buildings, there are several fine-grain layers in continuous alternation, including an organic clay layer with a varying thickness of 5–10 m, organic clayey silt to silt layer, 5–10 m thick, and a clayey sand to sand layer with a thickness of 2–3 m (Figure 4b). The organic clay layer contains a significant amount of plant residue and limestone fragments. Investigations of the soil formations in the greater Messolonghi area [53] revealed that the clay layers are rich in shell and biogenic particles. The content of organic material in the clay layers is significant, ranging from 5 to 13%. In several locations in the city, the organic clay horizon is located above the water level, thus manifesting in the oxidation of the layer's organic content.

According to the geological maps by the Hellenic Survey of Geology and Mineral Exploration (HSGME), the Pliocene deposits have a thickness of 80–100 m. Underlying that formation is the flysch with a thickness of 1200–1400 m, followed by the Paleocene and Senonian limestone with a thickness of 300–400 m.

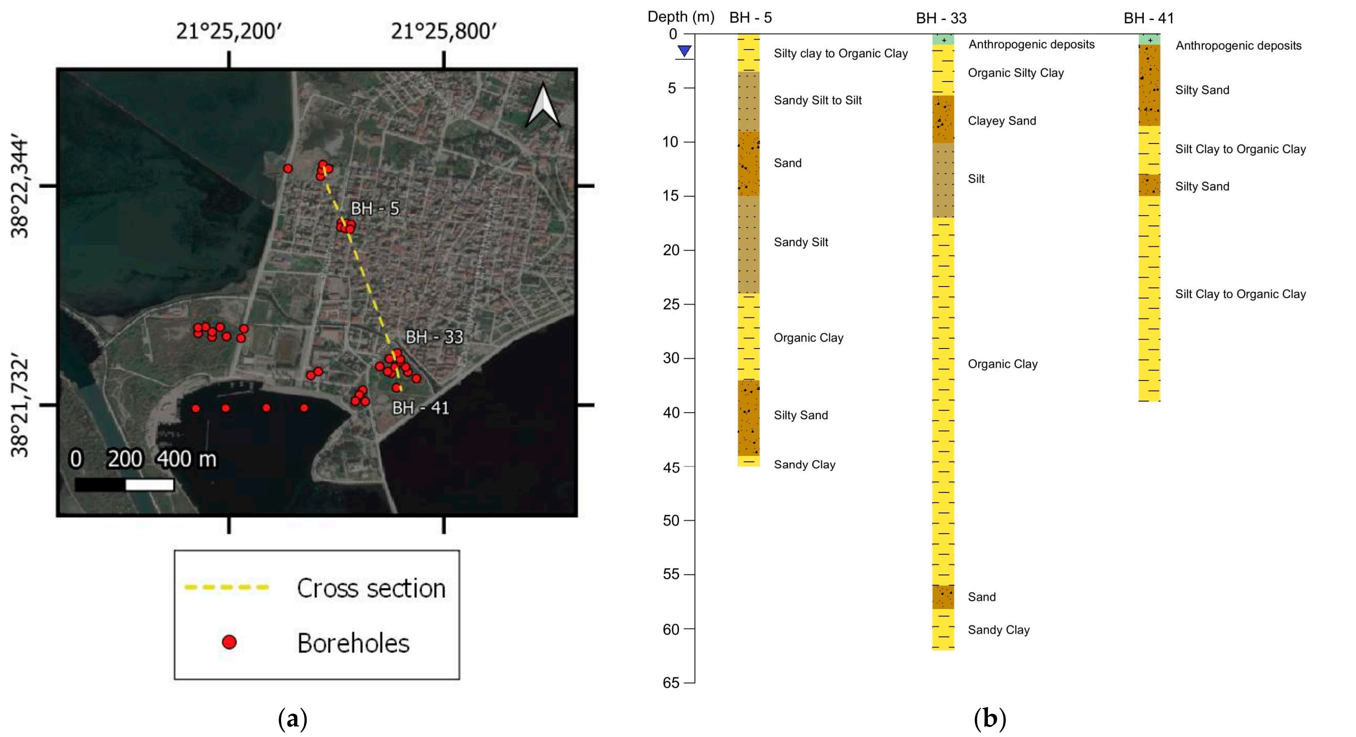

Figure 4. (**a**) Geotechnical borehole locations in Messolonghi (**b**) Indicative logs along the cross section of (**a**).

2.2. Geotechnical Setting

A total of 44 drilling profiles (Figure 4a) and over 100 oedometer tests were collected for the city of Messolonghi from the Hellenic Survey of Geology and Mineral Exploration [54,55], the Central Laboratory of Public Works [56,57] archives, and private geotechnical consultants' reports [58]. These data were analyzed and statistically processed, and they are presented in Tables 1 and 2. Data for all the layers are provided in Tables S1 and S2.

Table 1. Physical and mechanical properties of Clayey Silt, Clay and Clayey Sand foundation formations of Messolonghi.

	Clayey Silt			Organic Clay			Clayey Sand		
	Unified Soil Classification System (USCS) Classification								
	SL			CL			ML		
	Min	**Average**	**Max**	**Min**	**Average**	**Max**	**Min**	**Average**	**Max**
	Physical Parameters								
Liquid Limit, LL (%)	29	33.1	38.1	24.9	36.01	49.7	-	-	-
Plasticity Limit, PL (%)	18	19.8	21	12	18.94	27.7	-	-	-
Sat. unit weight, γ (kN/m^3)	17.4	19.2	21.6	18.5	19.5	20.3	-	20.3	-
	Mechanical Parameters								
Initial void ration, e	0.69	0.86	1.07	0.56	0.8	1	-	0.86	-
Compression index, C_c	0.222	0.276	0.3	0.23	0.282	0.328	-	-	-
UC Strength, q_u (kPa)	-	-	-	-	61.9	-	-	-	-
	Shear Box Test								
Cohesion, c (kN/m^2)	1.89	7.82	17.76	8.54	20.9	33.3	-	39.08	-
Friction angle, φ	3.7	13	22.1	19.1	21.6	24.1	-	40	-
	Standard Penetration Test								
N_{SPT}	7	7	8	3	8	18	-	13	-

Table 2. Minimum, mean and maximum depth.

	Min	**Average**	**Max**
Depth	5	27.2	100

According to the test results, all layers detected in the study area are highly compressible, presenting high to very high compression index (C_c) values ranging from 0.187 to 0.467. Additionally, as indicated by the low standard penetration test values (N_{SPT}), they can be described as very soft to moderately stiff. For instance, the organic clay layers of the coastal deposits, constituting most of the formations, can be identified with SPT values between 3 and 18.

2.3. Hydrogeological Setting

In the broader Messolonghi area, there are two aquifer systems, a karstic aquifer system within the Alpine–pre-Alpine bedrock formations (Pc-Ek and Ks.k) and the one developed in the Quaternary formations (Figure 4), occupying the wider plane area extending west of Messolonghi.

The shallow unconfined aquifer recharges by both lateral karstic water overflow along the foothill and through the scree and by filtration of surface water, which fluctuates due to the mean sea level rise. Nonetheless, previous boreholes indicated the mean groundwater level inside the city of Messolonghi at around 2 m below the surface (Figure 3). According to the groundwater contour lines (Figure S1, Table S3), the aquifer flows from the foothills of the Arakynthos mountain, behind the study area, and to the south–southwest toward the coastline. This aquifer also recharges the permeable phase of the flysch. A previous hydrochemical study [53] has identified increased salinity in the groundwater toward the coastline, which can be related to seawater intrusion and possibly the dissolution of the salt content of the sediments.

In Aitolikon, the hydrogeological conditions are predictable. The lagoon water penetrates the earth fill material, and the groundwater level can be identified as 1.0 to 1.5 m under the ground, at the sea surface level.

3. Sea Level Rise and Annual Precipitation Rates

The recent escalation of global warming and climate change has led to an increase in abnormal global weather patterns and extreme hydrological phenomena. In the case of Messolonghi and Aitolikon, these phenomena have frequently resulted in natural disasters such as floods. Thus, climate change has increased the frequency and volume of precipitation in the study area (Figure S2) and caused a sea level rise.

With the aid of satellite altimetry, numerous studies and research projects [59–65] have been conducted concerning the sea level rise in European coastal areas, with varying results. According to Marcos et al., 2016 [66], the Mediterranean Sea experienced an average sea level rise of 2.6 $\pm$ 0.2 mm/year between 1993 and 2015. In most coastal regions of Europe, the Copernicus Climate Change Service [67] estimated that the rising sea level values from 1993 to 2021 were in the range of 2–4 $\pm$ 0.9 mm/year, while the NOAA/STAR Laboratory for Satellite Altimetry has calculated a mean value of 2.2 $\pm$ 0.4 mm/year [68]. These findings are consistent with the Katakolon tidal gauge (Figure S3), located 81 km from the study area, which recorded a 2.09 mm/year sea level rise from 1970 to 2021, adding up to a total increase of 11 cm since the 1970s [69,70]. However, the tidal gauge in Patras' port (Figure S3), 32 km from the study area, recorded a higher sea level rise in the gulf of 7 mm/year from 2017 to 2021. (Table S4, Figure S4) [70]. The fact that the Patras' dataset refers to a short time period reduces its accuracy. Nevertheless, the finding makes it clear that the sea level is rising. The continuous sea level rise can be interpreted as one of the main causes for the reported rush of seawater over the lowlands.

The Representative Concentration Pathway (RCP) and Shared Socioeconomic Pathways (SSP) scenarios can be used to estimate the projected sea level rise. RCPs describe different levels of greenhouse gases and other radiative forcings that might occur in the future. Four pathways were developed, covering a broad spectrum of forcing in 2100 (RCP 2.6, RCP 4.5, RCP 6.0, and RCP 8.5 watts per meter squared). However, the RCP scenarios did not include socioeconomic factors and their change over the next century. These factors were examined in the SSPs and included variables such as population, economic growth, education, urbanization, and the rate of technological development. They evaluated five different ways in which the world might evolve in the absence of climate policy and how various levels of climate change alleviation can be achieved when the mitigation goals of RCPs and SSPs are combined. Figure 5 shows the projected mean sea level rise for coastal Greece and the Messolonghi lagoon based on these scenarios.

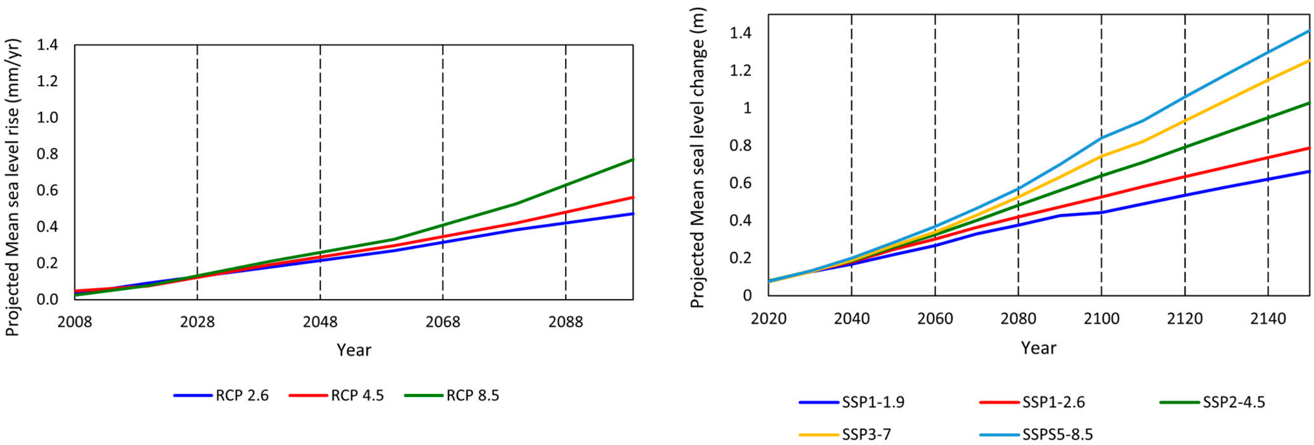

(**a**) (**b**)

Figure 5. (**a**) Projected Mean Sea level change in coastal Greece according to RCP scenarios [71] (**b**). Projected Mean Sea level change at Messolonghi lagoon according to the SSP scenarios [72].

The RCP2.6 model, the lowest baseline emissions scenario, indicates a 0.5 m mean sea level rise of coastal Greece over the next 80 years, while RCP 8.5, the highest baseline emissions scenario, indicates 0.77 m [71]. If a very high-emissions scenario (SSP5-8.5) is considered, then the mean sea level in the Messolonghi lagoon is expected to rise to 0.85 m by 2100 [72].

The constant increase in the sea level has been causing a rush of seawater over the Messolonghi and Aitolikon lowlands. The situation is expected to worsen over the next few years because of the gradual subsidence of the sites and the increase in the mean precipitation rates caused by climate change. The sections of Messolonghi and Aitolikon that could be flooded by 2100, considering only the elevation of the locations, are presented in Figure 6. These maps were created using FloodMap [73]. A sea level rise of 85 cm (SSP5–8.5/worst case scenario) and a natural sediment compaction of 15 cm [74] were both taken into account.

The precipitation data obtained from the automatic weather stations' NOANN network of the National Observatory of Athens (NOA) [75] for the Aitolikon weather station were statistically processed and analyzed to obtain the mean monthly and yearly precipitation rates. For the examined period (2015–2022), monthly rainfall values varied from 0 to 357 mm, while the average annual precipitation was 750 mm/yr. The most significant rainfalls were mainly concentrated between October and February, where the average precipitation rate was 133 mm. As mentioned, rainfalls were significantly high during the wet period, leading to difficulties in draining river flow discharge and increased water levels. The maximum inundated area has increased each year because of the intensification of the precipitation volume and the rising sea level, causing several floods (Figure 7). It should be mentioned that both researchers and the Ministry of Citizen Protection have designated Messolonghi and Aitolikon as the zones of potentially high flood risk [74] and, in 2015 and 2019, they were declared as areas in a state of emergency due to flooding.

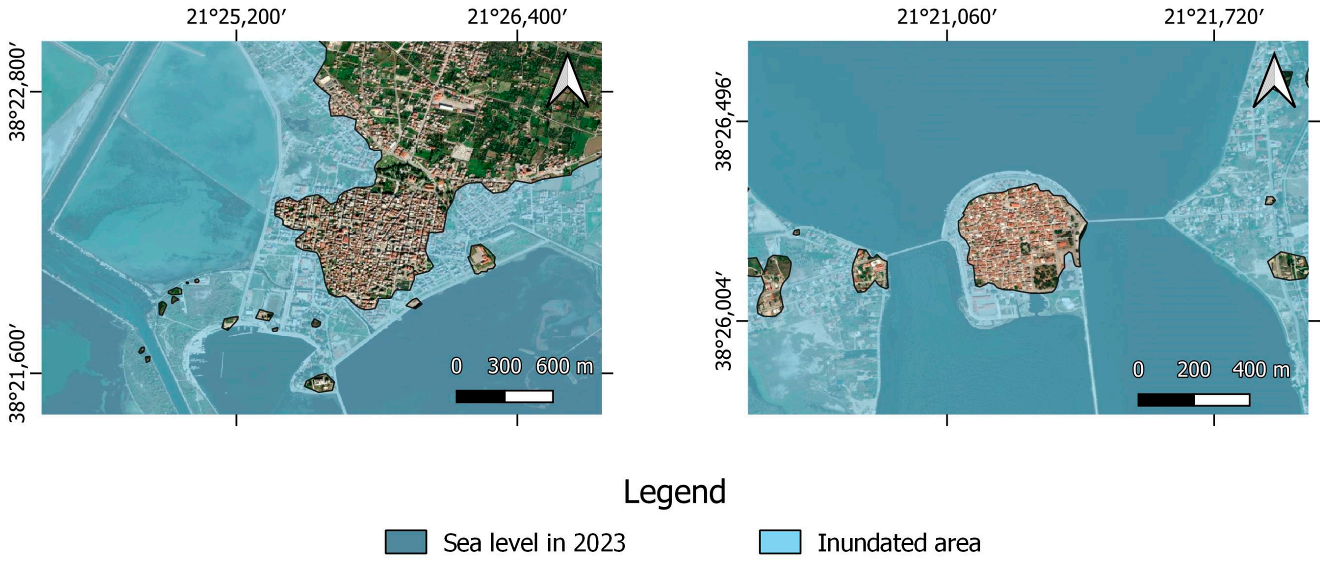

(**a**) (**b**)

Figure 6. (**a**) Flooded sections of Messolonghi in 2100 according to SSP5-8.5 sea level assumption (**b**) Flooded sections of Aitolikon in 2100 according to SSP5-8.5 sea level assumption.

(**a**) (**b**) (**c**)

Figure 7. (**a**) Flooded Messolonghi—extreme events of 3 December 2021 [76] (**b**) Flooded Aitolikon—extreme events of 4 August 2015 [77] (**c**) Flooded Aitolikon—extreme events of 26 September 2020 [78].

4. Multi-Temporal InSAR Analysis and PSI Results

4.1. Methodology

For the present study, the Stanford Method for Persistent Scatterers (StaMPS) [79] was implemented on Sentinel-1 satellite data provided by the Hellenic Mirror Site and the Sentinel Greek Copernicus Data Hubs [80], enabling small-scale surface deformation monitoring over an extended period. Additionally, to reduce the atmospheric impact on the estimated LOS displacements, a phase-based linear correction was implemented on the produced Sentinel-1 interferograms using the open-source Toolbox for Reducing Atmospheric InSAR Noise (TRAIN) [81].

A total of 161 and 120 Sentinel-1A and 1B SLC images from the Copernicus program, of both descending and ascending satellite passes, were processed with the parallelized

Persistent Scatterer Interferometry (P-PSI) processing chain [49], developed in the unit BEYOND Center of EO Research and Satellite RS of the IAASARS/NOA. Information about the SAR datasets employed in the current study is provided in Table 3. The estimated line-of-sight (LOS) displacements provided insights into the considerable continuing hazard in the areas of interest. A previous analysis with Multitemporal Sar Interferometry was also performed in the greater study area, but no detailed interpretation of the aforementioned phenomenon was provided [82]. Vertical displacements were estimated using Equation (1) for both the ascending and descending track and were compared to the results presented by the Copernicus European Ground Motion Service [83,84].

$$v_{vertical} = \frac{v_{LOS}}{cos\theta} \quad (1)$$

where for every scatterer $v_{vertical}$ is the vertical displacement, v_{LOS} is the Line-Of-Sight displacement and θ is the incidence angle

Table 3. Data information.

Sensor	Satellite Pass	Path-Frame	No. of Images	No. of Permanent Scatterers	Temporal Coverage	Primary Image
Sentinel 1A/1B	Descending	80–463	163	160,819	11 November 2015–21 December 2021	12 April 2019
	Ascending	175–119	120	49,378	13 August 2015–13 February 2022	22 June 2018

The standard deviation values for the descending and ascending track are displayed in Figure S5a,b, respectively.

Furthermore, the information provided by the European Ground Motion Service (EGMS) was evaluated. The EGMS is the largest wide-area A-DInSAR service ever conceived. This initiative was defined in the period 2016–2017 and finalized in 2017. The same year, it was approved by the Copernicus user forum and the Copernicus committee. The EGMS aims to provide reliable information regarding natural and anthropogenic ground motion phenomena over Europe for the study of geohazards and human-induced deformation such as slow-moving landslides, subsidence due to groundwater exploitation or underground mining, volcanic unrests and many more. This goal is achieved through the use of Sentinel-1A and 1B SAR images, received from two different look angles (ascending and descending), with a revisit time of six days, processed at full resolution. The key elements of the European Ground Motion Service (EGMS) are stated in the White Paper, available online at https://land.copernicus.eu/user-corner/technical-library/egms-white-paper, accessed on 25 February 2022 [85]. EGMS is included in the Copernicus Land Monitoring Service [86].

4.2. Results

The PSI LOS displacements (Figure 8a,b) and vertical displacements (Figure 8c,d), revealed intensive ground motion changes in the narrow study areas of Messolonghi and Aitolikon, during the examined time period.

In order to evaluate and validate the spatial distribution of the subsidence, it was necessary to correlate it with ground truth data. The geological and geotechnical data acquired from maps, technical reports, and drilling profiles enabled the validation and interpretation of the PSI results, and thus, a more holistic and temporally complete view of the phenomenon was achieved.

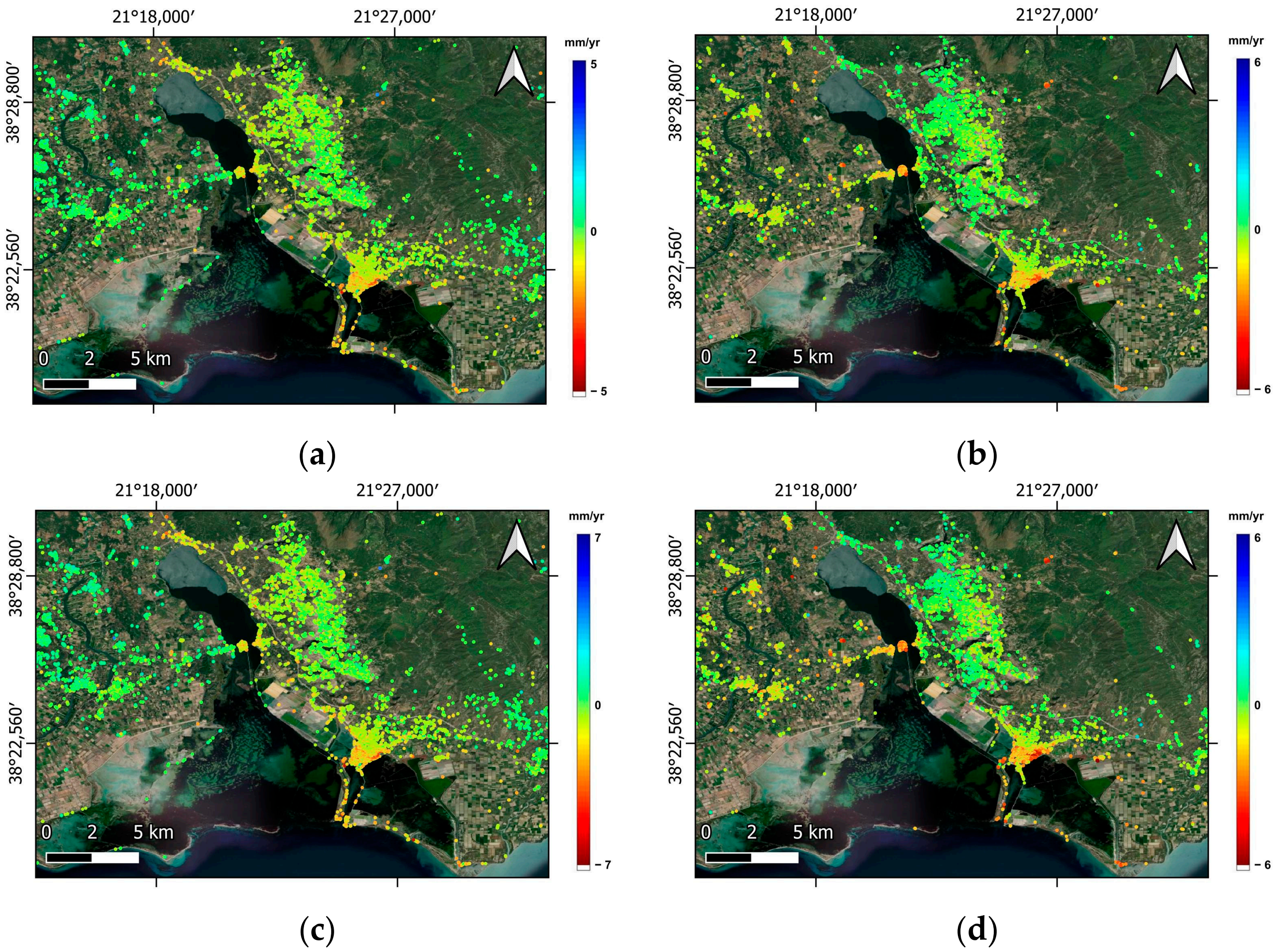

Figure 8. LOS displacements for the broader area of (**a**) the descending satellite pass (no. 80) (**b**) for the ascending satellite pass (no. 175). Vertical displacements for the broader area of (**c**) the descending satellite pass (no. 80) (**d**) for the ascending satellite pass (no. 175). All figures were derived from the P-PSI satellite data analysis conducted at BEYOND.

5. In Situ Data

Extensive field campaigns were carried out in both cities, where damage to several buildings was recorded. Numerous buildings were affected by the subsiding phenomena, including the Prefectural Administration of Aitoloakarnania, the Port Authority, the Public Finance Service of Messolonghi, and many residential buildings. Significant damages were found in the older buildings (Figure 9), throughout Messolonghi (Figure 13).

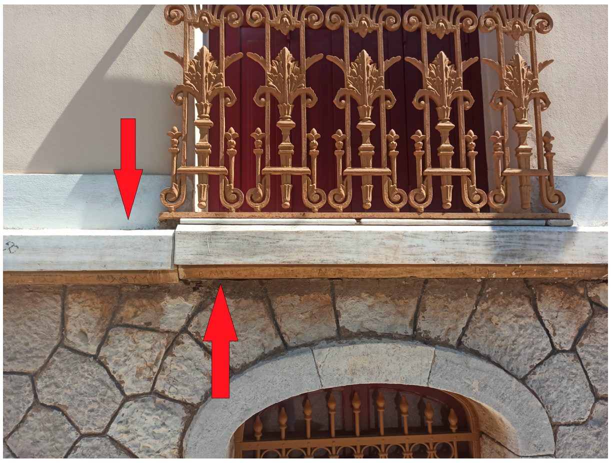
(**a**)

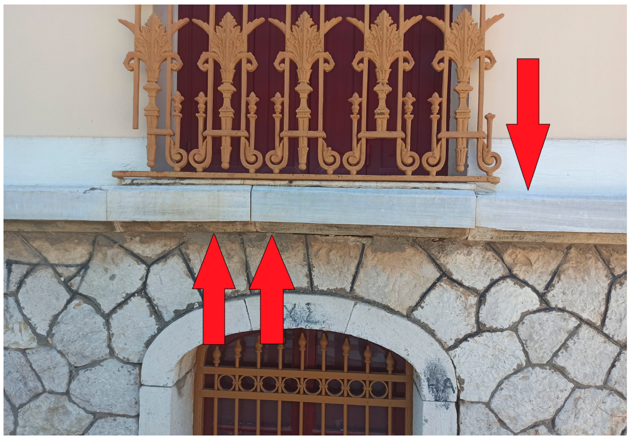
(**b**)


(**c**)

Figure 9. Damages recorded in buildings due to deferential deformations. (**a**) South side balcony damage in Building D (**b**) West side balcony damage in Building D (**c**) Balcony damage in Building E. Arrows indicate the movement trend due to subsidence.

6. Discussion

The objective of the present study was twofold: first, to identify and interpret the dominant mechanisms of the observed surface deformations, and second, to identify areas of significant movements. To successfully manage this task, all factors that may have affected the evolution of land subsidence phenomena have been evaluated (geological, geotechnical, and hydrogeological) using remote sensing data, sea rise data, and precipitation rates. Identifying and mapping ground displacements in Messolonghi and Aitolikon would enrich our knowledge of the deformation patterns of these areas and provide valuable insights for future research on subsiding phenomena in western Greece.

6.1. Messolonghi Ground Deformations

6.1.1. Deformation Values

The town of Messolonghi presents a variety of vertical deformation rates (Figure 10). Maximum displacement values in the vicinity of Messolonghi are of the order of −5 mm/yr. The Persistent Scatterers (PSs) indicated relatively stable ground conditions in the northern part of the town during the investigated time period as the vertical values ranged from 0.3 to 1.3 mm/year. However, the recorded deformations were increased in other parts of the town. Subsiding Persistent Scatterers were concentrated along the coastal zone, with a higher density east of the town (mean deformation rate of −5 mm/yr). The south and west parts of the town also presented a mean subsidence rate of −2.5 mm/yr and −3 mm/yr, respectively.

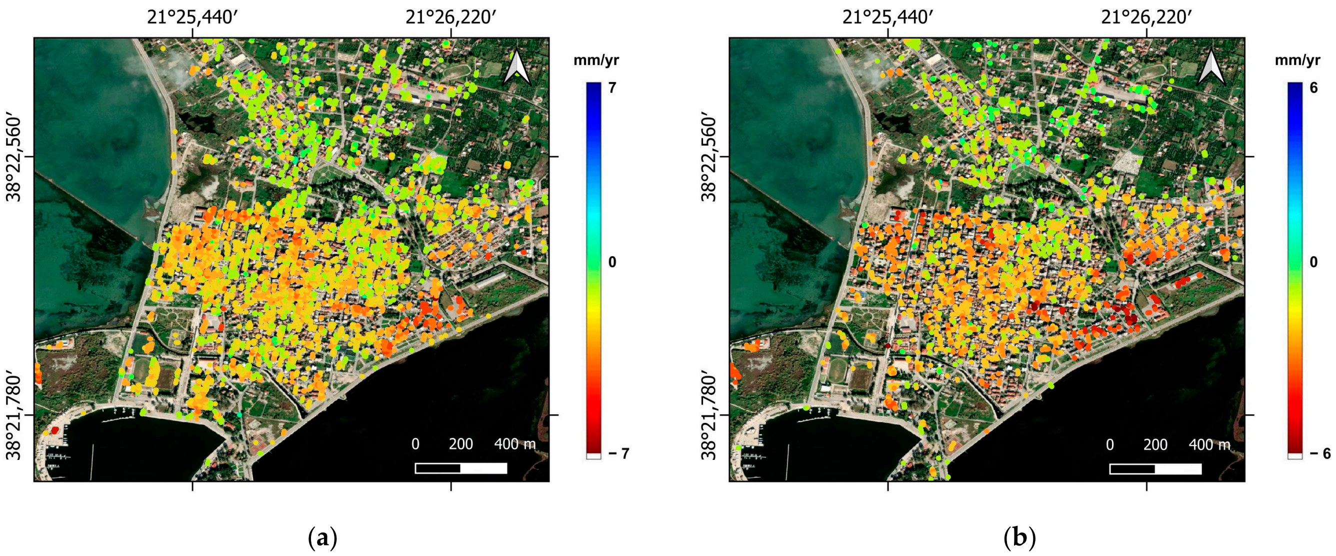

Figure 10. Spatial distribution of the Sentinel-1 vertical deformations in Messolonghi for (**a**) the descending satellite pass (no. 80) & (**b**) the ascending satellite pass (no. 175). Both coming from the P-PSI satellite data analysis conducted at BEYOND.

The mean vertical deformation rates provided by the Copernicus European Ground Motion Service (Figure 11) were around −4.5 mm/yr. The NOA analysis and the EGMS data were in perfect agreement as, in both datasets, the spatial distribution of the deformations was the same and the northern part of the town presented the highest deformation rates.

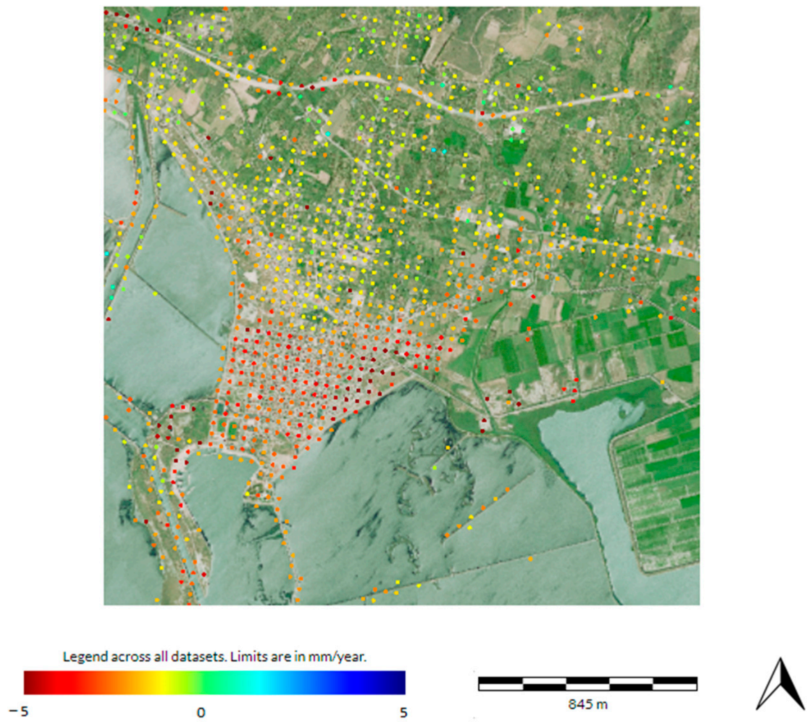

Figure 11. Vertical displacements from the European Ground Motion Service of Copernicus in Messolonghi.

6.1.2. Geotechnical Data Correlation

As indicated, the city is built on compressible soil, probably under consolidated formations subjected to subsidence caused by the external construction loads, leading to foundation settlement. Most buildings in Messolonghi are built with mat foundations and only a few with spread footings. Deformation patterns are manifested primarily in buildings constructed with the former type of foundation. Moreover, as mentioned, in several locations in the city, the organic clay layer is situated above the water level, resulting in subsidence and the oxidation of the layer's organic content.

Secondary consolidation might also be considered a factor leading to land subsidence in some parts of the study area, specifically the central part of Messolonghi. Even though the buildings in that area were constructed during the 1950s, vertical displacements still manifest today. It can be assumed that the primary consolidation was exhausted, and the secondary consolidation (creep) is now manifesting. However, a more likely explanation is that, due to the constant increase in the sea level and the increased precipitation rates, the groundwater level fluctuates throughout the year, leading to the reactivation of the primary consolidation.

6.1.3. Precipitation Rate Correlation

The time series of the deformations referring to the PSs located on almost all the damaged buildings follow a specific pattern. At the beginning of the wet season (October–November), the deformations appear to slow down, and they start accelerating at the end of the dry season (August–September). It seems that the recharge of the aquifers during the wet period (from September to June) increased the groundwater pore pressure and, with a short time offset from the beginning of the rainfalls, led to the deceleration of the subsidence. Conversely, the draining of the aquifers during the dry period (July to September) reduced the groundwater pore pressure leading to the acceleration of the deformations, also with a short time offset from the beginning of the draining. The time offset, in either case, was not fixed, depending on the intensity of the rainfalls or the severity of the pumping activities that occurred each year.

The above described deformation pattern and its correlation with the precipitation can be witnessed at Figure 12a referring to a PS located on Building B (Figure 13a). This graph isolates the vertical displacements as provided by the European Ground Motion Service of Copernicus.

The graph in Figure 12b refers to the vertical deformations from BEYOND's P-PSI satellite data analysis. These datasets are less sensitive to the fluctuation in the vertical deformations, and as a result, only the constant subsiding trend is visible in both descending and ascending track time series.

The above discussion proves that the natural recharge of the aquifers caused a slight alteration in the deformation trends of the land subsidence, decelerating the deformations. Nevertheless, it is clear that the seasonal fluctuation of the groundwater head could not affect the overall continuous subsiding trend witnessed through the time series.

6.1.4. Underground Water Exploitation

To determine whether the aquifer has been subjected to overexploitation during the past years, the groundwater level measurements conducted during the hydrological year (October 2005–April 2006) [53] were compared with measurements conducted by the HSGME from 2015 to 2022. As presented in Figure S6, the monitoring boreholes included in the current HSGME network [87] are insufficient for producing new groundwater level contour maps, referring to the recent measurements (2015–2022). So, measurements from neighboring boreholes of the two networks were compared to arrive at a conclusion concerning the possibility of an extensive groundwater discharge.

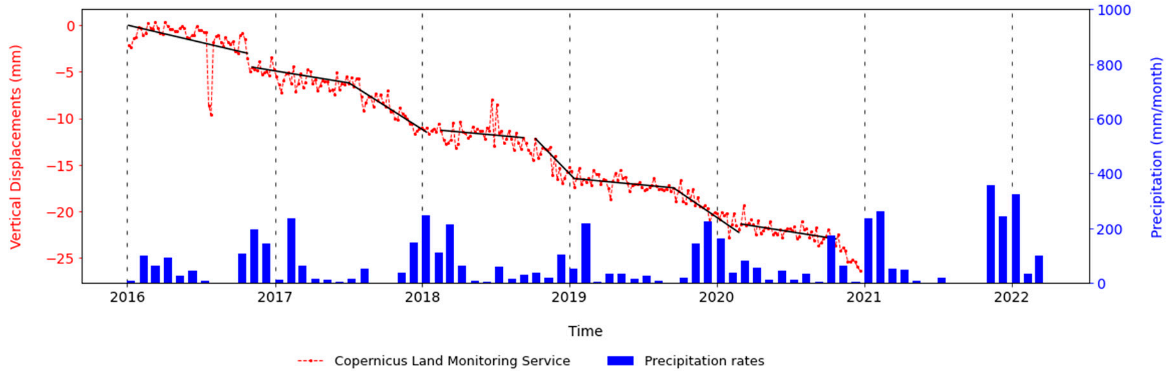

(**a**)

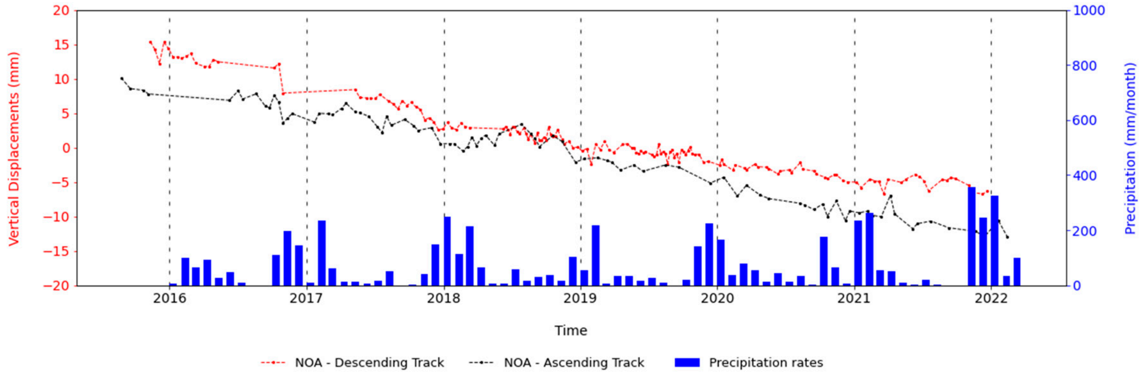

(**b**)

Figure 12. Displacements recorded vs. precipitation rates for the Prefectural Administration of Aitoloakarnania building (B). Each blue bar represents the precipitation rates for 1 month (B) (**a**) Vertical displacements in the form of time-series from the European Ground Motion Service of Copernicus. Trend lines (black color) indicate the changes on the subsidence rate (**b**) Vertical deformations for the descending and ascending track from BEYOND's P-PSI satellite data analysis.

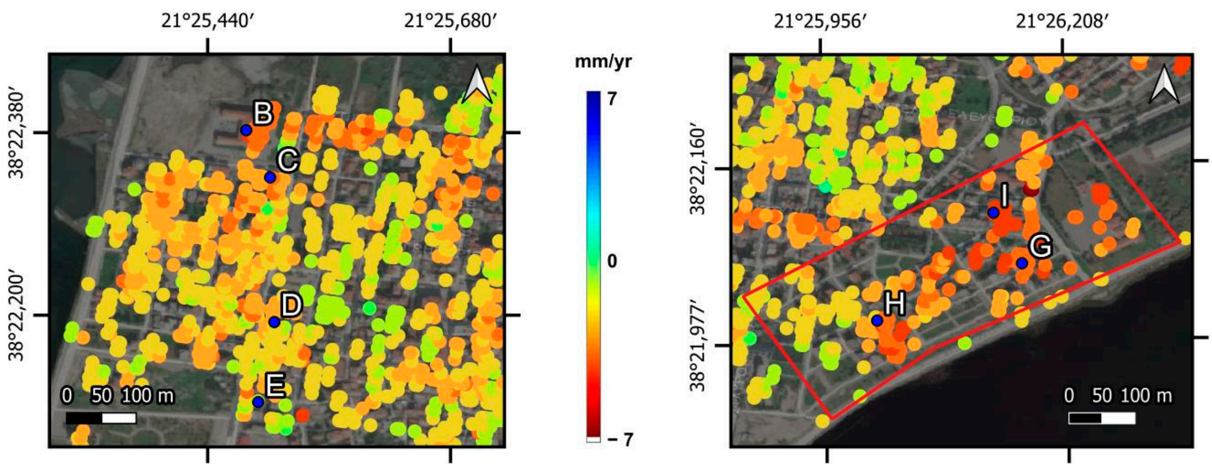

(**a**) (**b**)

Figure 13. (**a**) West Messolonghi, Locations of buildings with recorded damages. Prefectural Administration of Aitoloakarnania (B), Port Authority (E) and Public Finance Service of Messolonghi (E) (**b**) East Messolonghi, the area with the most significant deformations (descending satellite pass no. 80). Letters B, C, D, E, H, I and G indicate the location of the buildings where damages were recorded.

By comparing the measurements conducted at the neighboring boreholes W5 and EL04250402 (Figure S7a), it is clear that the groundwater level has remained practically stable since 2005. In particular, in both boreholes, the groundwater head fluctuated between 25 and 30 m during the 2005–2006 hydrological year and since 2015. The same conclusion can be reached for the measurements conducted at the boreholes W11 and EL04090402 (Figure S7b), where the groundwater head fluctuated between 6 and 8.5 m during both periods mentioned above.

Following the above discussion, it can be concluded that there is no deformation, due to the overexploitation of the aquifers currently at this particular site.

6.1.5. Land Use Correlation

According to Corine's land use map for 2006 [88] and 2018 [89] (Figure 14), there has been an increase in the area used for residential and commercial purposes in Eastern Messolonghi. The areas used for residential purposes are referred in Figure 14 legend as "Continuous urban fabric" and "Discontinuous urban fabric", and for commercial purposes as "Industrial and commercial units" and "Sport and leisure facilities". The correlation between the land usage map and the vertical deformations from the descending track is presented in Figure S8. This change supports the findings of the P-PSI analysis, which indicated that the affected area's subsidence rate, is the highest in the greater area of Messolonghi, as already mentioned. Due to the recent construction of the buildings in that area, it was possible to record the deformations imposed, by their loads. An increase of the areas used for industrial and commercial purposes is also visible in the eastern section of Messolonghi, which extends towards the national road. The PS points demonstrate how the deformation induced by the exploitation of the underground water and building loads, is now beginning to manifest.

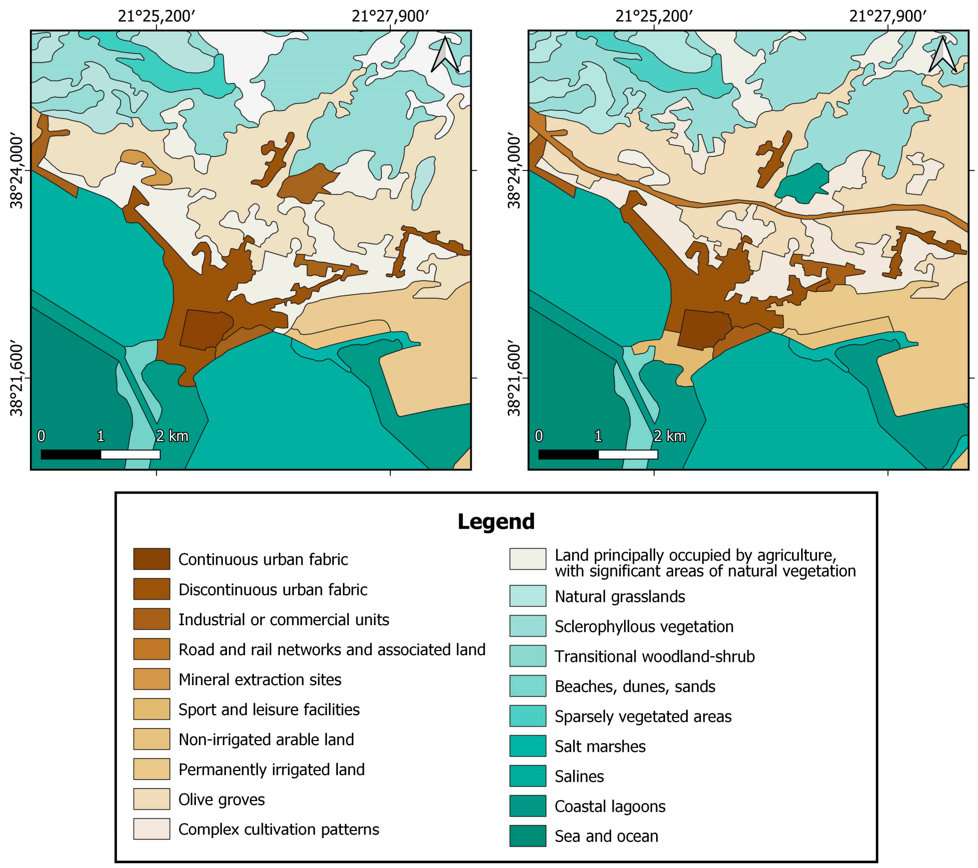

Figure 14. Land use for the greater area of Messolonghi in (**a**) 2006 and in (**b**) 2018.

6.1.6. Tectonic Correlation

As shown in Figure 3, the rock background and faults are located behind the study area. Greece is a highly tectonic zone, and earthquakes have occurred throughout the examined time period. Nonetheless, they were only up to a magnitude of 4 A, and the faults located behind the study area did not become active. Subsidence caused by the earthquakes would have been evident in the time series as a sharp step after the event. Thus, subsidence cannot be attributed to tectonic causes.

6.1.7. Similar Case Studies

From the above discussion, it can be concluded that the subsidence in Messolonghi can be attributed to the compaction of the Holocene deposits, common in stream and river deltas. Existing literature and case studies dealing with the same topic [18–20] verify these findings. The rate of subsidence recorded in these studies ranges between −3 and −15 mm/year. There is a slight difference between the values presented in these case studies and the ones calculated for Messolonghi (−3 to −5 mm/year), and it could be explained by a variety of reasons, including building loads, time of construction, and in what era the delta was formed.

6.2. Aitolikon Ground Deformations

6.2.1. Deformation Values

In Aitolikon, maximum vertical deformation values reach a mean rate of −4 mm/yr (Figures 15 and 16). Significant damages to buildings M, N, and L (Figure 17a) have been recorded in the northern part of the town. It is worth mentioning that in that area, the houses' foundations were constructed in the water before the addition of the 1969 filling. The highest deformations were observed in the southern part of the island, where the Vaso Katraki Museum (O in Figure 17a) is located (mean values of −4.5 mm/year). The museum was constructed on top of the 1969 reclaimed area.

(**a**)

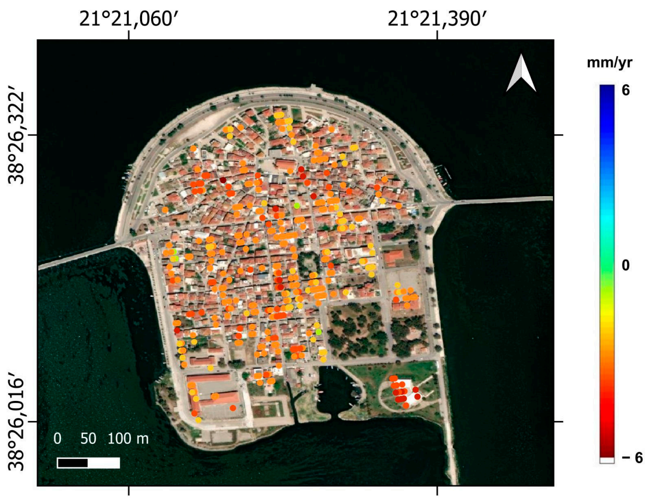

(**b**)

Figure 15. Spatial distribution of the Sentinel-1 vertical deformations in Aitolikon for (**a**) the descending satellite pass (no. 80) & (**b**) the ascending satellite pass (no. 175). Both coming from the P-PSI satellite data analysis conducted at BEYOND.

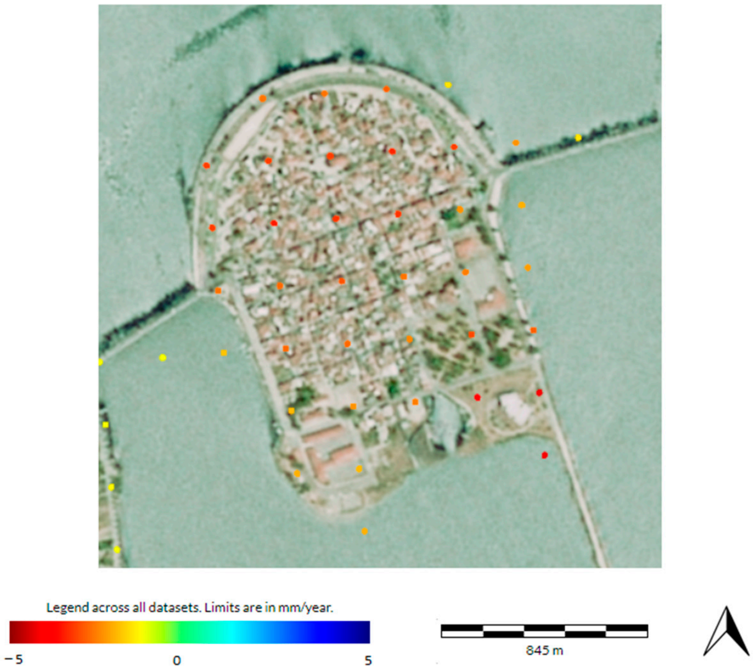

Figure 16. Vertical displacements from the EGMS of Copernicus in Aitolikon.

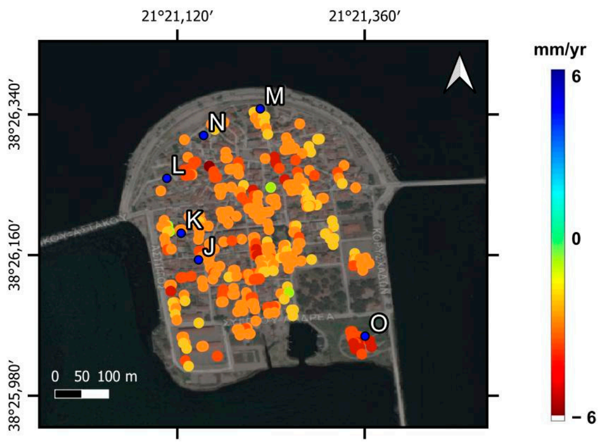

(**a**)

(**b**)

Figure 17. (**a**) Locations of buildings with recorded damages in Aitolikon. Vaso Katraki Museum's location is represented as O (**b**) Building M—Balcony damage (South side of Aitolikon). Letters J, K, L, M, N, O indicate the location of the buildings where damages were recorded.

6.2.2. Underground Water Exploitation

The time series of the deformations referring to the PSs located on almost all the damaged buildings indicate a continuous subsiding trend. At this particular site, sessional fluctuations related to the changes in the groundwater head, identical to those identified in Messolonghi, are not visible. The continuous subsiding trend can be viewed from the Copernicus European Ground Motion Service dataset and the P-PSI satellite data analysis conducted at BEYOND. The continuously subsiding deformation pattern can also be seen in Figure 18a, referring to the average rate of the PS located at Vaso Katraki Museum (O in Figure 17a). This graph isolates the vertical displacements provided by the Copernicus European Ground Motion Service. The graph in Figure 18b refers to the vertical deformations obtained by BEYOND's P-PSI satellite data analysis for the ascending track.

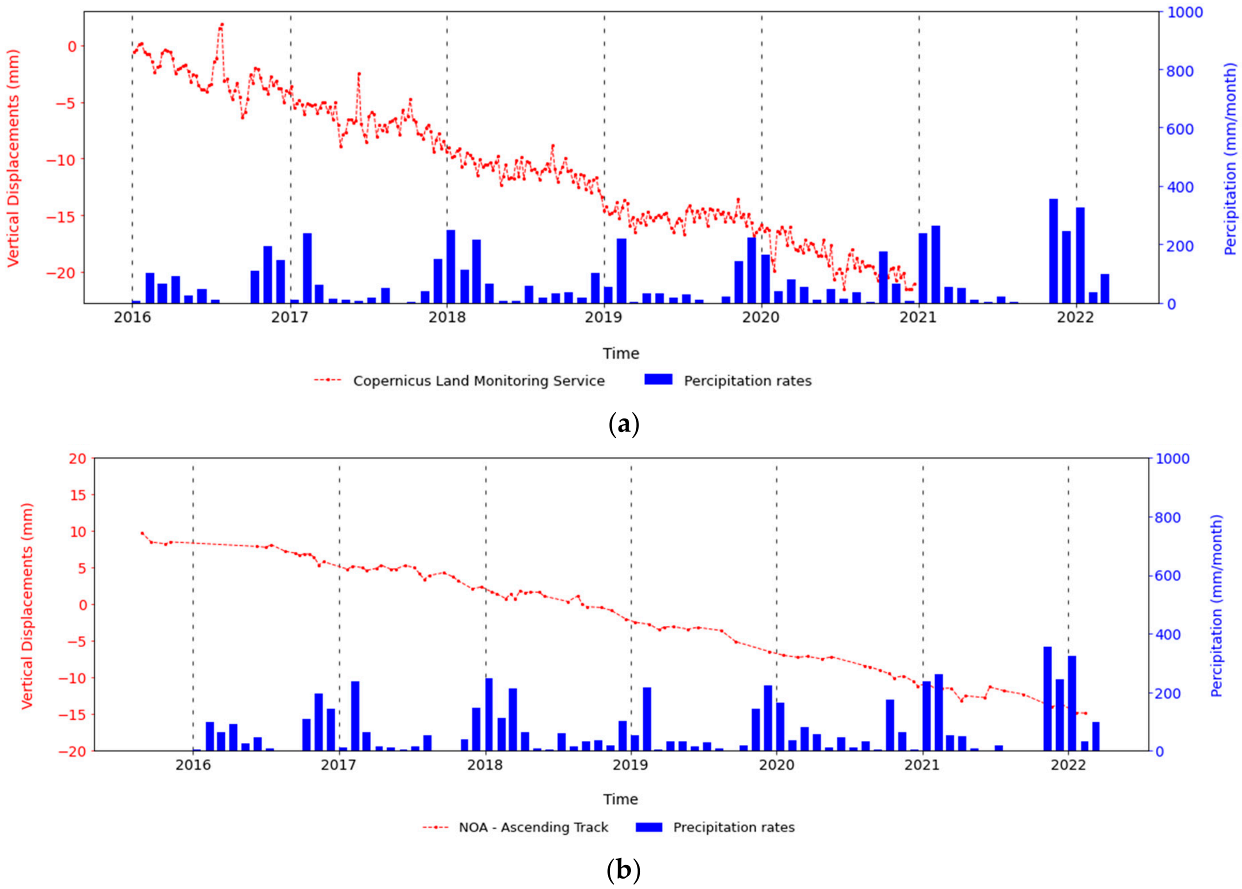

Figure 18. Displacements recorded vs. precipitation rates for Vaso Katraki Museum (O). Each blue bar represent the precipitation rates for 1 month (**a**) Vertical displacements time-series from the European Ground Motion Service of Copernicus (**b**) Vertical displacements time-series for the Vaso Katraki Museum (O) for the ascending satellite pass from BEYOND's P-PSI satellite data analysis.

As no productive drills are exploiting the groundwater underneath Aitolikon, it is clear that the observed groundwater head fluctuation less than 1 m, due to the variations in the level of the lake, is not sufficient to affect the subsiding trend.

6.2.3. Geotechnical Data Correlation

Unfortunately, geotechnical data referring to the geotechnical setting of Aitolikon are not available. Nevertheless, the fact that the entire city is founded over randomly deposited artificial fill leaves no doubt about the high compressibility of the formations leading to subsidence due to natural and external loads-induced compaction. It should also be mentioned that different motion rates were observed for nearby buildings, possibly caused by the different foundation types used and the heterogeneity of the filling materials. Following the above discussion, it is clear that the only cause of the land subsidence at Aitolikon is the natural compaction and the compaction due to the external loads exerted by the constructions.

7. Conclusions

The study areas were the coastal cities of Messolonghi and Aitolikon. Both sites have been subjected to land subsiding phenomena where significant building damage has been reported. The present study provides an approach for identifying the subsidence mechanism by combining the geotechnical characteristics, hydrogeological data, sea level data, and precipitation data and verifying the displacements using space-borne SAR interferometry (InSAR) techniques and ground truth data. As observed, the subsiding deformation trend cannot be attributed to the exploitation of the groundwater level or tectonic causes. The coastal deposits occupying most of the study area were proven to be compressible due to the low compression index (C_c) values identified in all surface soil layers. Therefore, primary consolidation was the key factor leading to the land subsidence phenomena. On the other hand, sea level rise and precipitation rates, which have increased over the past few years due to climate change, are crucial factors that play a significant role in the repeated flooding of both coastal cities. The manifestation of the deformations was verified using the space-borne SAR interferometry techniques conducted by the unit BEYOND Centre for Earth Observation Research and Satellite Remote Sensing of IAASARS/NOA and the Copernicus European Ground Motion Service. The results of the InSAR techniques were validated through field trips conducted in the affected areas, where building damage was documented.

The current research offers an interesting case study of two coastal cities affected by land subsidence caused primarily by the consolidation of the compressible soil layers. At the same time, the two coastal towns are affected by the constant sea level rise and a consequent rush of seawater. The situation is expected to worsen over the next few years, considering the combined effect of the gradual subsidence of the sites and the intensification of the meteorological phenomena caused by climate change.

Supplementary Materials: The following supporting information can be downloaded at: https://www.mdpi.com/article/10.3390/rs15082112/s1, Figure S1. Ground water level contour lines for (a) October 2005 and (b) April 2006. Produced by evaluating the raw data coming from the study of Lemesios (2006) [42]; Figure S2. Monthly precipitation rates recorded by the Aitolikon weather station [63]. Each blue bar represent the precipitation rates for 1 month; Figure S3. Patra and Katakolon tidal gauges locations; Figure S4. Patra's tidal gauge timeseries; Figure S5. Standard deviation values for the (a) descending & (b) ascending track; Figure S6. The location of the boreholes used by Lemesios (2006) [42] at 2005–2006 (yellow dots) and since 2015 by HSGME (red dots) [72]; Figure S7. (a) Ground water level for boreholes EL04250402 and W5 (b) Ground water level for boreholes EL04090402 and W11; Figure S8. (a) Land use for the greater area of Messolonghi in 2006 and descending track LOS displacements (b) Land use for the greater area of Messolonghi in 2018 and descending track LOS displacements; Table S1. Physical and mechanical properties of Silt and Silty Sand foundation formations of Messolonghi; Table S2. Physical and mechanical properties of Silty Clay and Sandy Clay foundation formations of Messolonghi; Table S3. Hydrogeological boreholes data from HSGME and Lemesios (2006); Table S4. Patras tidal gauge data for the 2017–2022 period [59].

Author Contributions: Conceptualization, N.A.; Validation, S.A., C.L. and C.K.; Formal analysis, N.A.; Investigation, S.A. and C.L.; Resources, C.L. and C.K.; Data curation, N.A. and S.A.; Writing—original draft, N.A.; Writing—review & editing, S.A., C.L. and C.K.; Visualization, N.A.; Supervision, C.L.; Project administration, C.L. All authors have read and agreed to the published version of the manuscript.

Funding: This research received no external funding.

Institutional Review Board Statement: Not applicable.

Informed Consent Statement: Not applicable.

Data Availability Statement: The datasets used and/or analysed during the current study are available from the authors upon request.

Acknowledgments: This research was supported by the "COLLABORATIVE DATA HUB RELAY FRAMEWORK ESA" Contract No. 4000138881/22/I-NS-bgh with National Observatory of Athens (NOA). The authors would like to acknowledge the European Land Monitoring Service of the European Environment Agency for freely providing the INSAR data.

Conflicts of Interest: The authors declare no conflict of interest.

References

1. Solari, L.; Del Soldato, M.; Bianchini, S.; Ciampalini, A.; Ezquerro, P.; Montalti, R.; Raspini, F.; Moretti, S. From ERS 1/2 to Sentinel-1: Subsidence Monitoring in Italy in the Last Two Decades. *Front. Earth Sci.* **2018**, *6*, 149. [CrossRef]
2. Osmanoğlu, B.; Dixon, T.H.; Wdowinski, S.; Cabral-Cano, E.; Jiang, Y. Mexico City subsidence observed with persistent scatterer InSAR. *Int. J. Appl. Earth Obs. Geoinf.* **2011**, *13*, 1–12. [CrossRef]
3. Cigna, F.; Osmanoğlu, B.; Cabral-Cano, E.; Dixon, T.H.; Ávila-Olivera, J.A.; Garduño-Monroy, V.H.; DeMets, C.; Wdowinski, S. Monitoring land subsidence and its induced geological hazard with Synthetic Aperture Radar Interferometry: A case study in Morelia, Mexico. *Remote Sens. Environ.* **2012**, *117*, 146–161. [CrossRef]
4. Gambolati, G.; Putti, M.; Teatini, P.; Gasparetto Stori, G. Subsidence due to peat oxidation and impact on drainage infrastructures in a farmland catchment south of the Venice Lagoon. *Environ. Geol.* **2006**, *49*, 814–820. [CrossRef]
5. Hoogland, T.; van den Akker, J.J.H.; Brus, D.J. Modeling the subsidence of peat soils in the Dutch coastal area. *Geoderma* **2012**, *171–172*, 92–97. [CrossRef]
6. Caramanna, G.; Ciotoli, G.; Nisio, S. A review of natural sinkhole phenomena in Italian plain areas. *Nat. Hazards* **2008**, *45*, 145–172. [CrossRef]
7. Galve, J.P.; Gutiérrez, F.; Lucha, P.; Guerrero, J.; Bonachea, J.; Remondo, J.; Cendrero, A. Probabilistic sinkhole modelling for hazard assessment. *Earth Surf. Process. Landf.* **2009**, *34*, 437–452. [CrossRef]
8. Ding, H.; Chen, S.; Chang, S.; Li, G.; Zhou, L. Prediction of Surface Subsidence Extension due to Underground Caving: A Case Study of Hemushan Iron Mine in China. *Math. Probl. Eng.* **2020**, *2020*, 5086049. [CrossRef]
9. Gambolati, G.; Teatini, P. Numerical Analysis of Land Subsidence Due to Natural Compaction of the Upper Adriatic Sea Basin. In *CENAS—Coastline Evolution of the Upper Adriatic Sea Due to Sea Level Rise and Natural and Anthropogenic Land Subsidence*; Gambolati, G., Ed.; Water Science and Technology Library: Dordrecht, The Netherlands, 1998; Volume 28, pp. 103–131, ISBN 978-94-011-5147-4. [CrossRef]
10. Kaitantzian, A.; Loupasakis, C.; Tzampoglou, P.; Parcharidis, I. Ground Subsidence Triggered by the Overexploitation of Aquifers Affecting Urban Sites: The Case of Athens Coastal Zone along Faliro Bay (Greece). *Geofluids* **2020**, *2020*, 8896907. [CrossRef]
11. Loupasakis, C.; Rozos, D. Finite-Element Simulation of Land Subsidence Induced by Water Pumping in Kalochori Village, Greece. *Q. J. Eng. Geol. Hydrogeol.* **2009**, *42*, 369–382. [CrossRef]
12. Galloway, D.L.; Burbey, T.J. Review: Regional Land Subsidence Accompanying Groundwater Extraction. *Hydrogeol. J.* **2011**, *19*, 1459–1486. [CrossRef]
13. Pacheco-Martínez, J.; Hernandez-Marín, M.; Burbey, T.J.; González-Cervantes, N.; Ortíz-Lozano, J.Á.; Zermeño-De-Leon, M.E.; Solís-Pinto, A. Land Subsidence and Ground Failure Associated to Groundwater Exploitation in the Aguascalientes Valley, México. *Eng. Geol.* **2013**, *164*, 172–186. [CrossRef]
14. Ezquerro, P.; Guardiola-Albert, C.; Herrera, G.; Fernández-Merodo, J.A.; Béjar-Pizarro, M.; Bonì, R. Groundwater and Subsidence Modeling Combining Geological and Multi-Satellite SAR Data over the Alto Guadalentín Aquifer (SE Spain). *Geofluids* **2017**, *2017*, 1359325. [CrossRef]
15. Tzampoglou, P.; Loupasakis, C. Numerical Simulation of the Factors Causing Land Subsidence Due to Overexploitation of the Aquifer in the Amyntaio Open Coal Mine, Greece. *HydroResearch* **2019**, *1*, 8–24. [CrossRef]
16. Buffardi, C.; Barbato, R.; Vigliotti, M.; Mandolini, A.; Ruberti, D. The Holocene Evolution of the Volturno Coastal Plain (Northern Campania, Southern Italy): Implications for the Understanding of Subsidence Patterns. *Water* **2021**, *13*, 2692. [CrossRef]
17. Bruno, L.; Campo, B.; Costagli, B.; Stouthamer, E.; Teatini, P.; Zoccarato, C.; Amorosi, A. Factors controlling natural subsidence in the Po Plain. *Proc. Int. Assoc. Hydrol. Sci.* **2020**, *382*, 285–290. [CrossRef]
18. Teatini, P.; Tosi, L.; Strozzi, T. Quantitative evidence that compaction of Holocene sediments drives the present land subsidence of the Po Delta. *J. Geophys. Res.* **2011**, *116*, B08407. [CrossRef]
19. Meckel, T.A.; Brink, U.S.; Williams, S.J. Current subsidence rates due to compaction of Holocene sediments in southern Louisiana. *Geophys. Res. Lett.* **2006**, *33*, L11403. [CrossRef]
20. Tornqvist, T.E.; Wallace, D.J.; Storms, J.E.A.; Wallinga, J.; Van Dam, R.L.; Blaauw, M.; Derksen, M.S.; Klerks, C.J.W.; Meijneken, C.; Snijders, E.M.A. Mississippi Delta subsidence primarily caused by compaction of Holocene strata. *Nat. Geosci.* **2008**, *1*, 173–176. [CrossRef]
21. van Asselen, S.; Stouthamer, E.; van Asch, T.W.J. Effects of peat compaction on delta evolution: A review on processes, responses, measuring and modeling. *Earth-Sci. Rev.* **2009**, *92*, 35–51. [CrossRef]
22. Tosi, L.; Da Lio, C.; Donnici, S.; Strozzi, T.; Teatini, P. Vulnerability of Venice's Coastland to Relative Sea-Level Rise. *Proc. Int. Assoc. Hydrol. Sci.* **2020**, *382*, 689–695. [CrossRef]
23. Johnston, J.; Cassalho, F.; Miesse, T.; Ferreira, C.M. Projecting the Effects of Land Subsidence and Sea Level Rise on Storm Surge Flooding in Coastal North Carolina. *Sci. Rep.* **2021**, *11*, 21679. [CrossRef] [PubMed]
24. Nicholls, R.J.; Lincke, D.; Hinkel, J.; Brown, S.; Vafeidis, A.T.; Meyssignac, B.; Hanson, S.E.; Merkens, J.-L.; Fang, J. A Global Analysis of Subsidence, Relative Sea-Level Change and Coastal Flood Exposure. *Nat. Clim. Chang.* **2021**, *11*, 338–342. [CrossRef]
25. Solari, L.; Ciampalini, A.; Raspini, F.; Bianchini, S.; Moretti, S. PSInSAR Analysis in the Pisa Urban Area (Italy): A Case Study of Subsidence Related to Stratigraphical Factors and Urbanization. *Remote Sens.* **2016**, *8*, 120. [CrossRef]
26. Da Lio, C.; Tosi, L. Land Subsidence in the Friuli Venezia Giulia Coastal Plain, Italy: 1992–2010 Results from SAR-Based Interferometry. *Sci. Total Environ.* **2018**, *633*, 752–764. [CrossRef] [PubMed]

27. Ciampalini, A.; Solari, L.; Giannecchini, R.; Galanti, Y.; Moretti, S. Evaluation of Subsidence Induced by Long-Lasting Buildings Load Using InSAR Technique and Geotechnical Data: The Case Study of a Freight Terminal (Tuscany, Italy). *Int. J. Appl. Earth Obs. Geoinf.* **2019**, *82*, 101925. [CrossRef]
28. Yastika, P.E.; Shimizu, N.; Abidin, H.Z. Monitoring of Long-Term Land Subsidence from 2003 to 2017 in Coastal Area of Semarang, Indonesia by SBAS DInSAR Analyses Using Envisat-ASAR, ALOS-PALSAR, and Sentinel-1A SAR Data. *Adv. Space Res.* **2019**, *63*, 1719–1736. [CrossRef]
29. Papadopoulos, G.A.; Ganas, A.; Agalos, A.; Papageorgiou, A.; Triantafyllou, I.; Kontoes, C.; Papoutsis, I.; Diakogianni, G. Earthquake Triggering Inferred from Rupture Histories, DInSAR Ground Deformation and Stress-Transfer Modelling: The Case of Central Italy During August 2016–January 2017. *Pure Appl. Geophys.* **2017**, *174*, 3689–3711. [CrossRef]
30. Herrera-García, G.; Ezquerro, P.; Tomás, R.; Béjar-Pizarro, M.; López-Vinielles, J.; Rossi, M.; Mateos, R.M.; Carreón-Freyre, D.; Lambert, J.; Teatini, P.; et al. Mapping the Global Threat of Land Subsidence. *Science* **2021**, *371*, 34–36. [CrossRef]
31. Amato, V.; Aucelli, P.P.C.; Corrado, G.; Di Paola, G.; Matano, F.; Pappone, G.; Schiattarella, M. Comparing Geological and Persistent Scatterer Interferometry Data of the Sele River Coastal Plain, Southern Italy: Implications for Recent Subsidence Trends. *Geomorphology* **2020**, *351*, 106953. [CrossRef]
32. Sykioti, O.; Kontoes, C.C.; Elias, P.; Briole, P.; Sachpazi, M.; Paradissis, D.; Kotsis, I. Ground deformation at Nisyros volcano (Greece) detected by ERS-2 SAR differential interferometry. *Int. J. Remote Sens.* **2003**, *24*, 183–188. [CrossRef]
33. Parcharidis, I.; Kourkouli, P.; Karymbalis, E.; Foumelis, M.; Karathanassi, V. Time series synthetic aperture radar interferometry for ground deformation monitoring over a small scale tectonically active deltaic environment (Mornos, Central Greece). *J. Coast. Res.* **2013**, *29*, 325–338. [CrossRef]
34. Kontoes, C.; Loupasakis, C.; Papoutsis, I.; Alatza, S.; Poyiadji, E.; Ganas, A.; Psychogyiou, C.; Kaskara, M.; Antoniadi, S.; Spanou, N. Landslide Susceptibility Mapping of Central and Western Greece, Combining NGI and WoE Methods, with Remote Sensing and Ground Truth Data. *Land* **2021**, *10*, 402. [CrossRef]
35. Alatza, S.; Papoutsis, I.; Paradissis, D.; Kontoes, C.; Papadopoulos, G.A.; Raptakis, C. InSAR Time-Series Analysis for Monitoring Ground Displacement Trends in the Western Hellenic Arc: The Kythira Island, Greece. *Geosciences* **2020**, *10*, 293. [CrossRef]
36. Papoutsis, I.; Kontoes, C.; Paradissis, D. Multi-Stack Persistent Scatterer Interferometry Analysis in Wider Athens, Greece. *Remote Sens.* **2017**, *9*, 276. [CrossRef]
37. Kontoes, C.; Alatza, S.; Chousianitis, K.; Svigkas, N.; Loupasakis, C.; Atzori, S.; Apostolakis, A. Coseismic Surface Deformation, Fault Modeling, and Coulomb Stress Changes of the March 2021 Thessaly, Greece, Earthquake Sequence Based on InSAR and GPS Data. *Seismol. Res. Lett.* **2022**, *93*, 2584–2598. [CrossRef]
38. Alatza, S.; Papoutsis, I.; Paradissis, D.; Kontoes, C.; Papadopoulos, G.A. Multi-Temporal InSAR Analysis for Monitoring Ground Deformation in Amorgos Island, Greece. *Sensors* **2020**, *20*, 338. [CrossRef]
39. Ilia, I.; Loupasakis, C.; Tsangaratos, P. Land Subsidence Phenomena Investigated by Spatiotemporal Analysis of Groundwater Resources, Remote Sensing Techniques, and Random Forest Method: The Case of Western Thessaly, Greece. *Environ. Monit. Assess.* **2018**, *190*, 623. [CrossRef] [PubMed]
40. Tsangaratos, P.; Loupasakis, C.; Ilia, I. Ground Subsidence Phenomena in Frakadona, West Thessaly, Greece. In Proceedings of the Fifth International Conference on Remote Sensing and Geoinformation of the Environment (RSCy2017), Paphos, Cyprus, 6 September 2017; Volume 10444, pp. 149–157. [CrossRef]
41. Rozos, D.; Sideri, D.; Loupasakis, C.; Apostolidis, E. Land Subsidence Due to Excessive Ground Water Withdrawal. A Case Study from Stavros—Farsala Site, West Thessaly Greece. *Bull. Geol. Soc. Greece* **2010**, *43*, 1850–1857. [CrossRef]
42. Raspini, F.; Loupasakis, C.; Rozos, D.; Adam, N.; Moretti, S. Ground Subsidence Phenomena in the Delta Municipality Region (Northern Greece): Geotechnical Modeling and Validation with Persistent Scatterer Interferometry. *Int. J. Appl. Earth Obs. Geoinf.* **2014**, *28*, 78–89. [CrossRef]
43. Svigkas, N.; Papoutsis, I.; Constantinos, L.; Tsangaratos, P.; Kiratzi, A.; Kontoes, C.H. Land Subsidence Rebound Detected via Multi-Temporal InSAR and Ground Truth Data in Kalochori and Sindos Regions, Northern Greece. *Eng. Geol.* **2016**, *209*, 175–186. [CrossRef]
44. Svigkas, N.; Papoutsis, I.; Loupasakis, C.; Tsangaratos, P.; Kiratzi, A.; Kontoes, C.H. InSAR Time-Series Monitoring of Ground Displacement Trends in an Industrial Area (Oreokastro—Thessaloniki, Greece): Detection of Natural Surface Rebound and New Tectonic Insights. *Environ. Earth Sci.* **2017**, *76*, 195. [CrossRef]
45. Loupasakis, C.; Rozos, D. Land Subsidence Induced by the Overexploitation of the Aquifers in Kalochori Village—New Approach by Means of the Computational Geotechnical Engineering. *Bull. Geol. Soc. Greece* **2010**, *43*, 1219–1229. [CrossRef]
46. Svigkas, N.; Loupasakis, C.; Papoutsis, I.; Kontoes, C.; Alatza, S.; Tzampoglou, P.; Tolomei, C.; Spachos, T. InSAR Campaign Reveals Ongoing Displacement Trends at High Impact Sites of Thessaloniki and Chalkidiki, Greece. *Remote Sens.* **2020**, *12*, 2396. [CrossRef]
47. Raspini, F.; Loupasakis, C.; Rozos, D.; Moretti, S. Advanced Interpretation of Land Subsidence by Validating Multi-Interferometric SAR Data: The Case Study of the Anthemountas Basin (Northern Greece). *Nat. Hazards Earth Syst. Sci.* **2013**, *13*, 2425–2440. [CrossRef]
48. Raspini, F.; Bianchini, S.; Moretti, S.; Loupasakis, C.; Rozos, D.; Duro, J.; Garcia, M. Advanced Interpretation of Interferometric SAR Data to Detect, Monitor and Model Ground Subsidence: Outcomes from the ESA-GMES Terrafirma Project. *Nat. Hazards* **2016**, *83*, 155–181. [CrossRef]

49. Svigkas, N.; Loupasakis, C.; Tsangaratos, P.; Papoutsis, I.; Kiratzi, A.; Kontoes, C. A Deformation Study of Anthemountas Graben (Northern Greece) Based on in Situ Data and New InSAR Results. *Arab. J. Geosci.* **2020**, *13*, 518. [CrossRef]
50. Svigkas, N.; Papoutsis, I.; Loupasakis, C.; Tsangaratos, P.; Kiratzi, A.; Kontoes, C. Radar Space Measurements of the Deforming Trends at Northern Greece Resulting from Underground Water Activity. In *BT—Advances in Remote Sensing and Geo Informatics Applications*; El-Askary, H.M., Lee, S., Heggy, E., Pradhan, B., Eds.; Springer International Publishing: Cham, Switzerland, 2019; pp. 309–313. [CrossRef]
51. Raspini, F.; Loupasakis, C.; Rozos, D.; Moretti, S. Basin and Local Scale Detection of Ground Subsidence through Persistent Scatterer Interferometry: The Anthemountas Basin (Northern Greece) Case Study. *Bull. Geol. Soc. Greece* **2013**, *47*, 1510–1518. [CrossRef]
52. Papoutsis, I.; Kontoes, C.; Alatza, S.; Apostolakis, A.; Loupasakis, C. InSAR Greece with Parallelized Persistent Scatterer Interferometry: A National Ground Motion Service for Big Copernicus Sentinel-1 Data. *Remote Sens.* **2020**, *12*, 3207. [CrossRef]
53. Lemesios, I. Environmental Hydrogeological Survey of the Horizons of the Wider Area of the Municipality of Messolonghi in Relation to Its Natural Healing Resources. Master's Thesis, University of Patras, Patras, Greece, 2008. Available online: https://hdl.handle.net/10889/823 (accessed on 21 December 2022).
54. Hellenic Survey of Geology & Mineral Exploration (HSGME). *Geotechnical Investigation of the Foundations for the Construction of Worker's Households in the Areas of Messolonghi-Aitolikon I, II-Agrinio*; Technical Report; HSGME: Acharnes, Greece, 1987; p. 5244.
55. Hellenic Survey of Geology & Mineral Exploration (HSGME). *Geological Report on the Messolonghi Lagoon Drainage Projects*; Technical Report; HSGME: Acharnes, Greece, 1958; p. 564.
56. Central Laboratory of Public Works. *Messolonghi V—O.E.K.*; Technical Report; Ministry of the Environment, Urban Planning and Public Works: Athens, Greece, 1997; pp. 8.5–118.
57. Central Laboratory of Public Works. *Geotechnical Investigation in O.E.K. Site for the Construction of Worker's Households in Messolonghi (Messolonghi V)*; Technical Report; Ministry of the Environment, Urban Planning and Public Works: Athens, Greece, 1997; pp. 8.5–133.
58. Douveas, N.; Kavadia, D.; Papadopoulou, P. Geotechnical Foundation Conditions of Mesologion Swimming Pool Center. *Bull. Geol. Soc. Greece* **2007**, *40*, 1644–1651. [CrossRef]
59. Vignudelli, S.; Birol, F.; Benveniste, J.; Fu, L.L.; Picot, N.; Raynal, M.; Roinard, H. Satellite Altimetry Measurements of Sea Level in the Coastal Zone. *Surv. Geophys.* **2019**, *40*, 1319–1349. [CrossRef]
60. The Climate Change Initiative Coastal Sea Level Team. Coastal Sea Level Anomalies and Associated Trends from Jason Satellite Altimetry over 2002–2018. *Sci. Data* **2020**, *7*, 357. [CrossRef] [PubMed]
61. Legeais, J.F.; Meyssignac, B.; Faugère, Y.; Guerou, A.; Ablain, M.; Pujol, M.I.; Dufau, C.; Dibarboure, G. Copernicus Sea Level Space Observations: A Basis for Assessing Mitigation and Developing Adaptation Strategies to Sea Level Rise. *Front. Mar. Sci.* **2021**, *8*, 1668. [CrossRef]
62. Frederikse, T.; Landerer, F.; Caron, L.; Adhikari, S.; Parkes, D.; Humphrey, V.W.; Dangendorf, S.; Hogarth, P.; Zanna, L.; Cheng, L.; et al. The Causes of Sea-Level Rise since 1900. *Nature* **2020**, *584*, 393–397. [CrossRef]
63. Hamlington, B.D.; Frederikse, T.; Nerem, R.S.; Fasullo, J.T.; Adhikari, S. Investigating the Acceleration of Regional Sea Level Rise During the Satellite Altimeter Era. *Geophys. Res. Lett.* **2020**, *47*, e2019GL086528. [CrossRef]
64. Fasullo, J.T.; Nerem, R.S. Altimeter-Era Emergence of the Patterns of Forced Sea-Level Rise in Climate Models and Implications for the Future. *Proc. Natl. Acad. Sci. USA* **2018**, *115*, 12944–12949. [CrossRef]
65. Nerem, R.S.; Beckley, B.D.; Fasullo, J.T.; Hamlington, B.D.; Masters, D.; Mitchum, G.T. Climate-Change–Driven Accelerated Sea-Level Rise Detected in the Altimeter Era. *Proc. Natl. Acad. Sci. USA* **2018**, *115*, 2022–2025. [CrossRef]
66. Marcos, M.; Jorda, G.; Cozannet, G. Le Sub-Chapter 2.2.1. Sea Level Rise and Its Impacts on the Mediterranean. In *The Mediterranean Region under Climate Change: A Scientific Update*; IRD Éditions: Marseille, France, 2016; pp. 265–275, ISBN 9782709922203. [CrossRef]
67. Copernicus Climate Change Service. Sea Level | Copernicus. Available online: https://climate.copernicus.eu/climate-indicators/sea-level (accessed on 25 September 2022).
68. NOAA/NESDIS/STAR—Laboratory for Satellite Altimetry/Sea Level Rise. Sea Level Rise. Available online: https://www.star.nesdis.noaa.gov/socd/lsa/SeaLevelRise/LSA_SLR_timeseries.php (accessed on 25 September 2022).
69. European Environment Agency. Global and European Sea Level Rise. Available online: https://www.eea.europa.eu/ims/global-and-european-sea-level-rise (accessed on 25 September 2022).
70. Flanders Marine Institute (VLIZ). Intergovernmental Oceanographic Commission (IOC) (2022): Sea Level Station Monitoring Facility at VLIZ. Available online: https://www.ioc-sealevelmonitoring.org (accessed on 25 September 2022). [CrossRef]
71. Climate Change Knowledge Portal Greece. Sea Level Rise. Available online: https://climateknowledgeportal.worldbank.org/country/greece/impacts-sea-level-rise (accessed on 25 September 2022).
72. NASA. Sea Level Projection Tool—NASA Sea Level Change Portal. Available online: https://sealevel.nasa.gov/ipcc-ar6-sea-level-projection-tool (accessed on 27 September 2022).
73. FloodMap. Available online: https://www.floodmap.net (accessed on 10 October 2022).
74. Pavlopoulos, K. Greek Case Studies: The Implications of the Expected Sea Level Rise on the Low Lying Areas of Continental Greece in the Next Century. 2020. Available online: http://www.coastalwiki.org/wiki/Greek_case_studies:_The_implications_of_the_expected_sea_level_rise_on_the_low_lying_areas_of_continental_Greece_in_the_next_century (accessed on 10 January 2023).

75. Lagouvardos, K.; Kotroni, V.; Bezes, A.; Koletsis, I.; Kopania, T.; Lykoudis, S.; Mazarakis, N.; Papagiannaki, K.; Vougioukas, S. The Automatic Weather Stations NOANN Network of the National Observatory of Athens: Operation and Database. *Geosci. Data J.* **2017**, *4*, 4–16. [CrossRef]
76. Messolonghibylocals.com. Available online: https://messolonghibylocals.com/floodmessolonghi (accessed on 28 November 2022).
77. Agrinioculture.gr. Available online: https://www.agrinioculture.gr/2014/10/06/provlimata-apo-tin-kakokeria-stin-etoloakarnania (accessed on 28 November 2022).
78. AgrinioNews.gr. Available online: https://www.agrinionews.gr/aganaktisan-aitoliko-vrochi-kai-plimmyra (accessed on 28 November 2022).
79. Hooper, A.; Segall, P.; Zebker, H. Persistent Scatterer Interferometric Synthetic Aperture Radar for Crustal Deformation Analysis, with Application to Volcán Alcedo, Galápagos. *J. Geophys. Res.* **2007**, *112*, B07407. [CrossRef]
80. Hellenic Mirror Site and the Sentinel Greek Copernicus Data Hubs. Available online: https://sentinels.space.noa.gr (accessed on 5 December 2022).
81. Bekaert, D.P.S.; Walters, R.J.; Wright, T.J.; Hooper, A.J.; Parker, D.J. Statistical Comparison of InSAR Tropospheric Correction Techniques. *Remote Sens. Environ.* **2015**, *170*, 40–47. [CrossRef]
82. Gkartzou, E.; Parcharidis, I.; Karymbalis, E.; Drakatou, M.L. Multitemporal SAR Interferometry in the Messolonghi-Etoliko Natura 2000 Overlapping Deltas Area. In Proceedings of the Fringe 2015: Advances in the Science and Applications of SAR Interferometry and Sentinel-1 InSAR Workshop, Frascati, Italy, 23–27 March 2015; Ouwehand, L., Ed.; ESA Publication SP-731: Frascati, Italy. [CrossRef]
83. Crosetto, M.; Solari, L.; Mróz, M.; Balasis-Levinsen, J.; Casagli, N.; Frei, M.; Oyen, A.; Moldestad, D.A.; Bateson, L.; Guerrieri, L.; et al. The Evolution of Wide-Area DInSAR: From Regional and National Services to the European Ground Motion Service. *Remote Sens.* **2020**, *12*, 2043. [CrossRef]
84. Costantini, M.; Minati, F.; Trillo, F.; Ferretti, A.; Novali, F.; Passera, E.; Dehls, J.; Larsen, Y.; Marinkovic, P.; Eineder, M.; et al. European Ground Motion Service (EGMS). In Proceedings of the International Symposium on Geoscience and Remote Sensing (IGARSS), Brussels, Belgium, 11–16 July 2021; pp. 3293–3296. [CrossRef]
85. EGMS White Paper. Available online: https://land.copernicus.eu/user-corner/technical-library/egms-white-paper (accessed on 25 February 2022).
86. CLSM. Available online: https://www.copernicus.eu/en/copernicus-services/land (accessed on 25 February 2022).
87. Groundwater Monitoring Network—DIPYN of HSGME. Available online: https://gaia.igme.gr/portal/apps/webappviewer/index.html?id=ba3251562a9f48dab498b8de2637afd3 (accessed on 28 November 2022).
88. © European Union. *Copernicus Land Monitoring Service 2006*; European Environment Agency (EEA): Copenhagen, Denmark, 2006.
89. © European Union. *Copernicus Land Monitoring Service 2018*; European Environment Agency (EEA): Copenhagen, Denmark, 2018.